AD-A127 287 RESEARCH ON THE CRYSTAL GROWTH AND DIELECTRIC 1/1
PROPERTIES OF HIGH PERMITTI..(U) ROCKWELL INTERNATIONAL
THOUSAND OAKS CA SCIENCE CENTER R R NEURGAONKAR MAR 83
UNCLASSIFIED SC5345.3AR N00014-81-C-0463 F/G 20/2 NL

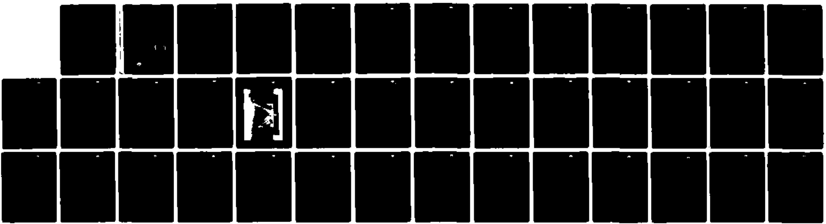

END
DATE
FILMED
5 -83
DTIC

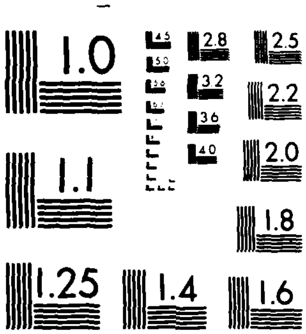
1.0
1.1
1.25
1.4
1.6
1.8
2.0
2.2
2.5
2.8
3.2
3.6
4.0

(12)

SC5345.3AR

SC5345.3AR

Copy No. 4

RESEARCH ON THE CRYSTAL GROWTH AND DIELECTRIC PROPERTIES OF HIGH PERMITTIVITY FERROELECTRIC MATERIALS

ANNUAL REPORT FOR THE PERIOD
March 1, 1982 through February 28, 1983

CONTRACT NO. N00014-81-C-0463
PROJECT NO. NR 032-609(471)

Prepared for

Office of Naval Research
800 North Quincy Street
Arlington, VA 22217

R.R. Neurgaonkar
Program Manager

MARCH 1983

Reproduction in whole or in part is permitted for any purpose of the United States Government.

Approved for public release; distribution unlimited

Rockwell International
Science Center

REPORT DOCUMENTATION PAGE

READ INSTRUCTIONS BEFORE COMPLETING FORM

1. REPORT NUMBER

2. GOVT ACCESSION NO. AD A127 287

3. RECIPIENT'S CATALOG NUMBER

4. TITLE (and Subtitle)
RESEARCH ON THE CRYSTAL GROWTH AND DIELECTRIC PROPERTIES OF HIGH PERMITTIVITY FERROELECTRIC MATERIALS

5. TYPE OF REPORT & PERIOD COVERED
Annual Technical Report
03/01/82 through 02/28/83

6. PERFORMING ORG. REPORT NUMBER
SC5345.3AR

7. AUTHOR(s)
R.R. Neugaonkar

8. CONTRACT OR GRANT NUMBER(s)
N00014-81-C-0463

9. PERFORMING ORGANIZATION NAME AND ADDRESS
Rockwell International Science Center
1049 Camino Dos Rios
Thousand Oaks, CA 91360

10. PROGRAM ELEMENT, PROJECT, TASK AREA & WORK UNIT NUMBERS
NR 032-609 (471)

11. CONTROLLING OFFICE NAME AND ADDRESS
Office of Naval Research
800 N. Quincy St.
Arlington, VA 22217

12. REPORT DATE
March 1983

13. NUMBER OF PAGES
40

14. MONITORING AGENCY NAME & ADDRESS(if different from Controlling Office)

15. SECURITY CLASS. (of this report)
Unclassified

15a. DECLASSIFICATION/DOWNGRADING SCHEDULE

16. DISTRIBUTION STATEMENT (of this Report)

Reproduction in whole or in part is permitted for any purpose of the United States Government.

Approved for public release; distribution unlimited.

17. DISTRIBUTION STATEMENT (of the abstract entered in Block 20, if different from Report)

18. SUPPLEMENTARY NOTES

19. KEY WORDS (Continue on reverse side if necessary and identify by block number)

Czochralski growth
Hot-pressing
BSKNN
PKLN
Lead barium niobate
Low frequency dielectric
Millimeter wave
Dielectric loss
Tungsten bronze

20. ABSTRACT (Continue on reverse side if necessary and identify by block number)

The systems investigated for potential millimeter wave applications are the stuffed tungsten bronze single crystal BSKNN, and the modified lead niobate ceramics PKLN and PBN. Low frequency and millimeter wave dielectric measurements show these materials to be promising for future applications. The observed high absorptive loss (tan $\delta \sim 0.2$) and rapidly decreasing permittivities at GHz frequencies for these initial samples may be due to piezoelastic coupling to heavily damped elastic waves through localized

defects. Work on the hot-pressed growth of PKLN and PBN ceramics shows this technique to be very promising for the enhancement of the dielectric properties of these lead-containing compositions, although cracking of PKLN is presently a problem due to its orthorhombic structure.

TABLE OF CONTENTS

Page

LIST OF ILLUSTRATIONS

LIST OF TABLES

1.0 INTRODUCTION AND PROGRESS SUMMARY

Over the past year the first phase of a systematic study of high permittivity ferroelectrics has been carried out, including the growth of single crystals, the preparation of ceramic samples, and dielectric characterization of these systems at both low frequency and millimeter wave frequencies (30 - 100 GHz). The behavior of ferroelectrics at frequencies in this latter range is largely unexplored, and presents an opportunity to test models based on soft modes, relaxors, or other mechanisms. Also, there is a need for components to act as control elements in millimeter wave radar systems, which could be met by high permittivity ferroelectrics if they retain the high sensitivity to applied electric fields and moderate intrinsic loss which they often exhibit for frequencies below 1 MHz.

The systems investigated this year were the tungsten bronzes barium strontium potassium sodium niobate (BSKNN), lead potassium lanthanum niobate (PKLN), and lead barium niobate (PBN). In BSKNN, all 12- and 15- fold coordinated sites are filled, while in the simpler tungsten bronzes such as strontium barium niobate (SBN) they are not. The potential for fluctuation in site occupation during crystal growth is therefore much reduced in BSKNN, and one may expect that the influence of such fluctuations on the dielectric properties can be judged by comparing measurements for BSKNN with results obtained earlier on SBN. PKLN and PBN possess orthorhombic and tetragonal ferroelectric phases, depending upon composition. Near the morphotropic phase boundary, both the linear and nonlinear dielectric susceptibilities of these materials should be high.

High frequency dielectric data has been obtained on BSKNN single crystals and PKLN ceramics. All samples show a pattern similar to the results obtained on SBN and strontium potassium niobate (SKN): high absorptive loss ($\varepsilon''/\varepsilon' \sim 0.2$) and rapidly decreasing permittivites, suggesting that a major contributor to the polarizability is relaxing at GHz frequencies. Piezoelectric coupling to heavily damped elastic waves through localized defects is being explored as a possible source of the observed dispersion.

2.0 MILLIMETER WAVE APPLICATIONS

The inherent advantages of millimeter wave radar systems in terms of all-weather capability when compared to infrared and optical sensors, and reduced weight and size when compared to conventional microwave radars, have led to increased emphasis by defense agencies on the development of millimeter wave seekers for a broad spectrum of major weapons systems. Device requirements for such radar systems were recently identified at an ARO-sponsored workshop on Short Millimeter Wave Non-Reciprocal Materials and Devices. It was concluded that while considerable advances have been made in the areas of sources of radiation, mixers, detectors, and receivers, there is a lack of comparable progress in the areas of components such as reciprocal and non-reciprocal devices (e.g., phase shifters, isolators, and circulators) and electronic-scanning antennas. It was recognized that new device concepts should be explored, and better materials developed (ferroelectric, ferrimagnetic, and semiconducting) to support these concepts.

One concept which we have been investigating is phase shifting by means of the large nonlinear susceptibility of ferroelectric materials. Sensitivities (dn/dE) of the microwave refractive index approaching 10^{-4} meters/volt are predicted for simple proper ferroelectrics from Devonshire models for the dielectric properties. Such materials can be used either as single discrete phase-shifting components in waveguides or as planar dielectric lenses. In the latter case, linear variation of the applied electric field across the lens will produce a uniform deflection of the millimeter wave beam passing through the lens, permitting electronic scanning of the beam. In either case, losses in passing through the phase-shifting material must be kept low (~ 1 dB) and the magnitude of applied voltages should fall within an accessible range for small, lightweight systems.

3.0 MATERIAL SYSTEMS OF INTEREST

3.1 Tungsten Bronze Structural Family

Among oxide ferroelectrics, the very large family of tungsten bronze structure crystals offers a broad range of ferroelectric properties with the possibility of "fine tuning" the material response by composition manipulation, and is automatically of major interest. For the composition $Ba_{0.39}Sr_{0.61}Nb_2O_6$, earlier studies have permitted the development of a full Gibbs function, and there is early indication that the important higher order stiffness parameters of the prototype do not change markedly with cation make-up.

Preliminary calculations using this Gibbs function gives a value of $(\partial n_3/\partial E_3)$ at 20°C

$$\partial n_3/\partial E_3 \cong 2.5 \times 10^{-6}/Vm^{-1}$$

in reasonable accord with measurements at GHz frequencies.

In the ferroelectric phase, the response increases to

$$\partial n_3/\partial E_3 \cong 6 \times 10^{-5}/Vm^{-1}$$

at 50°C, and it will be interesting to see if this trend is confirmed by measurements.

Initial calculations for the biased quadratic response suggest that the sensitivity may be vastly improved by operation in this mode. At 82°C under a bias field of 1 Kv/cm, we calculate an induced linear response

$$\partial n_3/\partial E_3 \cong -5 \times 10^{-3}/Vm^{-1} \quad ,$$

more than 3 orders larger than the room temperature response. It must be noted, however, that the response is a strong function of both temperature and bias field in this mode; however, some high frequency measurements in this regime are clearly required.

A second family of bronze structure crystals which is of interest are the $(Na_xK_{1-x})_2(Ba_ySr_{1-y})_4Nb_{10}O_{30}$ compositions. In these crystals, all A_1 and A_2 sites in the structure are filled and there is some indication that the dielectric loss levels may be lower.

A third bronze family of interest is the $Pb_{1-x}Ba_xNb_2O_6$ compositions. In this system, increasing lead content leads to the appearance of an orthorhombic ferroelectric phase with a morphotropic phase boundary near the composition $Pb_{0.6}Ba_{0.4}Nb_2O_6$. The high transverse Curie point θ for tetragonal compositions near morphotropy leads to unusually high ϵ_{11} and d_{15} values, and thus to the possibility of large values of r^1_{11} and r^1_{15}.

3.2 Perovskite Structural Family

Single crystals of perovskite structure ferroelectrics are difficult to grow and process to single domain configuration. In all materials, both pure ferroelectric and partial ferroelastic:ferroelectric domains occur due to the very high symmetry (m3m) of the prototype paraelectric phase. Since Gibbs functions are available for $BaTiO_3$, $KNbO_3$, $KNb_{1-x}Ta_xO_3$ and $PbZr_{1-x}Ti_xO_3$ systems, we propose to calculate the dielectric saturation functions for the single domain states in these families. We do not, however, anticipate major advantage over the bronze structure family crystals.

The feature in the perovskite family which is, however, of major importance is the multiaxial character of the ferroelectric response which leads to interesting and useful dielectric, piezoelectric and electro-optic response in the ceramic form. For the polar ferroelectric phases, the complex domain structures, grain to grain constraints, the highly anisotropic nature of the single domain permittivity and the difficulty of processing to a perfect single phase assemblage may make interpretation of the response difficult. In the paraelectric phase, however, many of these difficulties are eliminated, and we expect that the quadratic response will be of more interest.

A characteristic of the ceramic which may be of significant interest in developing a high quadratic response at low applied voltage is the manner in which perovskite type ceramics may be processed to produce a highly reduced conducting grain structure, separated by an insulating grain boundary region. In $BaTiO_3$-based capacitors made by this type of processing, "effective permittivities" greater than 100,000 can be achieved, indicating field multiplication by a factor of 50 or more across the grain boundary region.

Since in a quadratic system the induced response varies as E^2, the field amplification factor A augments the optical path length by a factor proportional to A^2, while the relief of field over the bulk of the grain only reduces the path length by a factor 1/A. For conducting levels ~10 ohm-cm in the grain which should be adequate to provide short time constants for the application of bias field to the boundary region, the impedance of the grain at high microwave or millimeter wave frequencies would not be affected. In effect, the reduced grains then provide a simple method for intercalating "transparent" electrodes into the volume of the sample.

3.3 SbSI Family Materials

The uniaxial ferroelectric antimony sulphur iodide, together with bromide and selenide solid solutions, form another interesting family where the Gibbs function is known. Since it is difficult to raise the true Curie temperature beyond 18°C in this system, the primary interest is in the quadratic or biased quadratic mode. Initial calculations suggest that at 32.5°C, under bias of 4.5×10^3 volts/cm, the induced linear effect gives $(\partial n_3/\partial E_3)$ values of the order $10 \times 10^{-3}/Vm^{-1}$.

It would appear that the materials in this family have promising prospects and more detailed evaluation is certainly in order. A summary of ferroelectric data for SbSI and several tungsten bronze and perovskite compositions is given in Table I.

Table 1

Ferroelectric Data for the Tungsten Bronze and Perovskite Family Compositions

Composition	Structure	Curie Temp. (°C)	Dielectric Constants Ferroelectric	Dielectric Constants Anti-Ferroelectric	Electro-Optic Effects	Material Availability
$Sr_{.5}Ba_{.5}Nb_2O_6$	T.B.	125	500	---	Large	Crystals
$Pb_{1-x}Ba_xNb_2O_6$	T.B.	200-560	2000-4000	---	Large	Crystals + Disks
$Pb_{1-2x}K_xLa_xNb_2O_6$	T.B.	100-560	1000-3000	---	Large	Crystals + Disks
$Ba_{1.2}Sr_{.8}K_{.75}Sr_{.25}Nb_5O_{15}$	T.B.	180	250-500	---	Large	Crystals
$KTa_{.65}Nb_{.35}O_3$	P	12	8650	---	Large	Disks
$Pb_{.97}La_{.02}(Zr_{.66}Ti_{.09}Sn_{.25})O_3$	P	-160	500	1100	---	Disks
$Pb_{.97}La_{.02}(Sr_{.54}Ti_{.11}Sn_{.30})O_3$	P	-180	800	1200	---	Disks
$Pb_{.92}La_{.08}(Zr_{.80}Ti_{.20})O_3$	P	-190	1500	4000	Large	Disks
$Pb_{.88}La_{.08}(Zr_{.65}Ti_{.35})O_3$	P	130	2700	---	Large	Disks
$Pb_{.88}La_{.08}(Zr_{.70}Ti_{.30})O_3$	P	120	4400	---	Large	Disks
SbSI	S	25	---	---	Large	Crystal + Disks

T.B. - Tungsten bronze structural family
P - Perovskite structural family
S - SbSI - Orthorhombic structure
Disk - Sintered or hot-pressed ceramics.

4.0 TUNGSTEN BRONZE FAMILY: GROWTH AND CHARACTERIZATION

4.1 Introduction

The *tungsten bronze structure family* is one of the most extensive, versatile, and potentially useful families of oxygen octahedron based ferroelectrics. This structure family embraces more than 100 individual end member compositions, and a continuous solid solution is possible between many of these end members.[1,2,3] These oxides can be represented by the formulae $A_5B_{10}O_{30}$ and $A_6B_{10}O_{30}$, where A = Ba, Sr, Ca, Pb, Na, K, Li etc. and B = Nb or Ta, or both. The structure consists basically of a complex array of corner sharing distorted MO_6 octahedra arranged in such manner that there are three different types of interstice in between. This structure can be considered an intermediate structure between the perovskite and pyrochlore-type structures. There are two types of tungsten bronze structures:

* Filled Tungsten Bronze: This consists of 10 octahedra and 6-cages which are built up of four 15-coordinated sites and two 12-coordinated sites surrounded by the 10-octahedra. If B ions occupy the octahedra sites and A ions in remaining six sites, and compound is typically represented by the formula $A_6B_{10}O_{30}$. Here either A or B sites can be occupied by more than two kinds of ions;

* Unfilled Tungsten Bronze: If the binary system consists of A-oxide and B-oxide, the resulting structure can be represented by the formula $A_5B_{10}O_{30}$. Here the six A sites are occupied by 5 ions, leaving only one site vacant.

A summary of the structural sequences and ferroelectric behavior of some recently studied tungsten bronze phases is given in Table 2. Some cations play an important role in stabilizing the tungsten bronze structure in $A_6B_{10}O_{30}$ and $A_5B_{10}O_{30}$ - type compounds. It has been found in the present work that the introduction of an alkali ions on the A sites, for example K^+ and Na^+ in

Table 2

The Structural Sequences and Ferroelectric Behavior of the Various Tungsten Bronze Phases

Compound	Number of Transitions	Transition Sequences
$K_3Nb_5O_{13}F_2$	None	4/mmm Paraelectric/Paraelastic
$Sr_2KNb_5O_{15}$, $K_3Li_2Nb_5O_{15}$, $Ba_6Ti_2Nb_8O_{30}$	One	4mm → 4/mmm Ferroelectric → Paraelectric/Paraelastic Ferroelastic
$Sr_2K_{0.5}Li_{0.5}Nb_5O_{15}$	One	mm2 → 4/mmm Ferroelectric → Paraelectric Ferroelastic Paraelastic
$Pb_2KNb_5O_{15}$	One	mm2 → 4/mmm Ferroelectric → Paraelectric Ferroelastic Paraelastic
$Sr_2KTa_5O_{15}$	Two	mm2 → mmm → 4/mmm Ferroelectric → Paraelectric → Paraelectric Ferroelastic Ferroelastic Paraelastic
$Pb_{2.7}K_{0.56}Nb_{0.91}$ • $Ta_{4.15}O_{15}$	Two	mm2 → mmm → 4/mmm Ferroelectric → Paraelectric → Paraelectric Ferroelastic Ferroelastic Paraelastic
$Ba_2NaNb_5O_{15}$	Three	4mm → mm2 → 4mm → 4/mmm Ferroelectric → Ferroelectric → Ferroelectric → Paraelectric Paraelastic Ferroelastic Ferroelastic Paraelastic
$Ba_{2.14}Li_{0.71}$ $Nb_{2.5}Ta_{2.5}O_{15}$	Three	222 → mm2 → 42m → 4/mmm Antiferroelectric → Ferroelectric → Paraelectric → Paraelectric Ferroelastic Ferroelastic Paraelastic Paraelastic

$(BaSr)_5Nb_{10}O_{30}$ as $Ba_{2-x}Sr_xK_{1-y}Na_yNb_5O_{15}$, yields more stuffed and stable bronze structures, which we have found useful for reducing dielectric losses at millimeter wave frequencies. Another bronze system, $Pb_{1-2x}K_xLa_xNb_2O_6$, studied in the present work is based on the unfilled orthorhombic tungsten bronze structure of $PbNb_2O_6$. In this case the addition of the K^+ and La^{3+} ions have not only filled the 15 and 12-coordinated sites, but this addition considerably improves the dielectric and piezoelectric properties for this solid solution system. The growth of these bronze compositions and their structural and ferroelectric properties are discussed in the following sections.

4.2 Growth and Characterization of BSKNN Crystals

Barium potassium niobate, $Ba_2KNb_5O_{15}$, is a well-known ferroelectric tetragonal bronze composition and has been considered to be useful for high frequency and electro-optic studies. However, this composition has received very little attention since it melts incongruently. Our recent work on this system shows that the addition of Sr^{2+} for Ba^{2+} and Na^+ for K^+ as $Ba_{2-x}Sr_xK_{1-y}Na_yNb_5O_{15}$ has not only changed the congruency situation (compositions of interest are congruent melting), but has also improved the dielectric, piezoelectric and electro-optic properties of this solid solution system.

Recently, we studied the phase equilibria relation for this solid solution system and found that the compositions close to the $Ba_{1.2}Sr_{0.8}K_{0.75}Na_{0.25}Nb_5O_{15}$ region are congruent melting and appear to be suitable for the proposed research work. Although the growth of several different composition crystals from this system with varying x and y have been planned, the work in this report is confined to the growth of $Ba_{1.2}Sr_{0.8}K_{0.75}Na_{0.25}O_{15}$ (BSKNN) crystals.

Single crystals of BSKNN have been grown by the Czochralski technique from a platinum crucible. Although the lattice match between the bronze crystals SBN and BSKNN is not close, SBN crystals were used initially as seed material for the growth of BSKNN crystals. This proved to be successful in growing small crystals of BSKNN which then were used as seed material in subsequent experiments to grow bigger and better quality crystals. BSKNN single crystals as large as 0.7 to 1.1 cm in diameter and 3-4 cm long have now been grown. Current growth parameters are as follows:

Pulling Rate:	6-8 mm/hr
Rotation Rate:	5 rpm
Growth Direction:	Along the c-axis
Growth Temperature:	1480°C

All of the $Ba_{1.2}Sr_{0.8}K_{0.75}Na_{0.25}Nb_5O_{15}$ crystals to date have been grown using a platinum crucible with an oxygen atmosphere. The resulting crystals are optically transparent and essentially colorless in appearance.

Crystals grown along the c-axis are usually faceted, which is quite exceptional for the Czochralski grown crystals. Figure 1 shows a typical crystal grown along the c-axis. In the course of this study, it was clearly observed that the rate of crystallization along the c-axis was greater than those along other directions (100, 110, etc.). As shown in Fig. 2, the growth habit of this large unit cell bronze crystal is square with four well defined facets. It is also interesting to note that the growth habit for the smaller unit cell bronze compositions such as SKN or SBN is cylindrical and exhibit 24 well defined facets.

Dielectric measurements as a function of temperature and frequency (1 kHz-1 MHz) have been performed on (100) and (001) oriented single crystals of BSKNN using sputtered platinum electrodes; the results of these measurements are shown in Figs. 3 and 4. The Curie temperature T_c for the $Ba_{1.2}Sr_{0.8}K_{0.75}Na_{0.25}Nb_5O_{15}$ composition was found to be 203°C for both the (100) and (001) orientations, with a maximum dielectric constant value of greater than 18,000 at T_c for the (001) direction. Dielectric measurements on BSKNN sintered ceramics for Sr_x contents of $0.7 < x < 0.9$ show that T_c increases with decreasing Sr content, and that the Curie temperature is also affected by the ionic site preference between the 12- and 15-fold coordinated sites in the lattice. Further research into this area is currently in progress.

SC82-19103

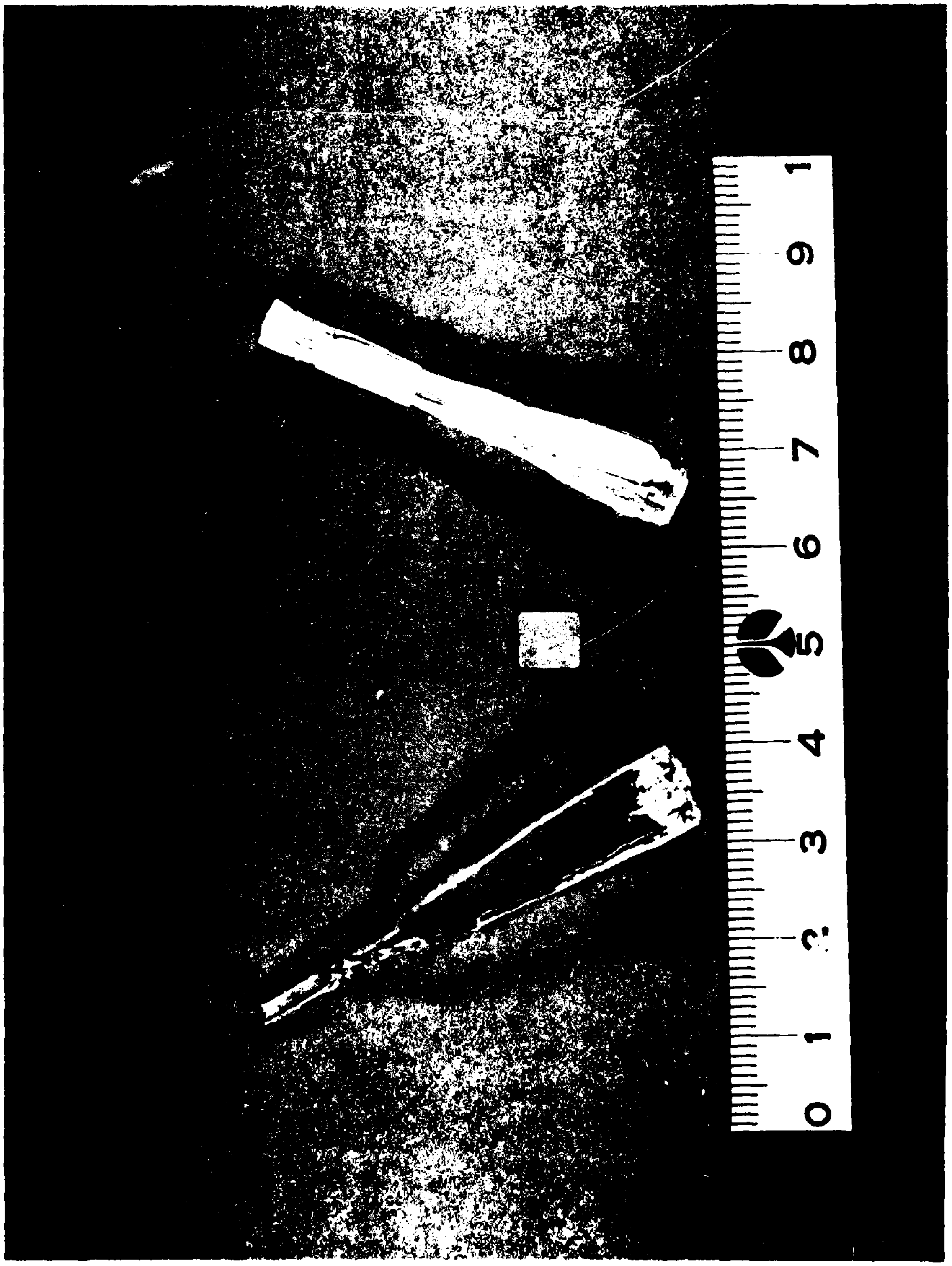

Fig. 1 Shows a typical 1 cm in diameter BSKNN single crystal grown along the C-axis.

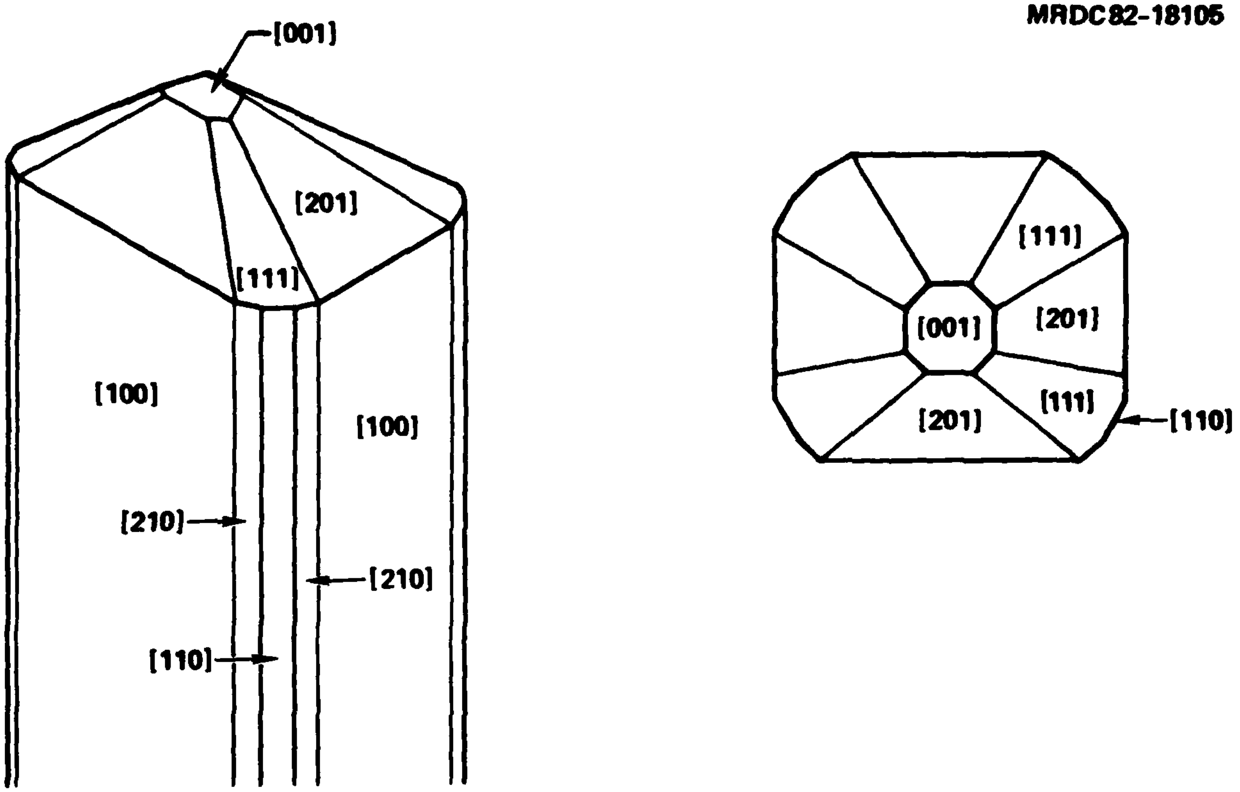

Fig. 2 Growth habit of large unit cell tungsten bronze crystals (BSKNN).

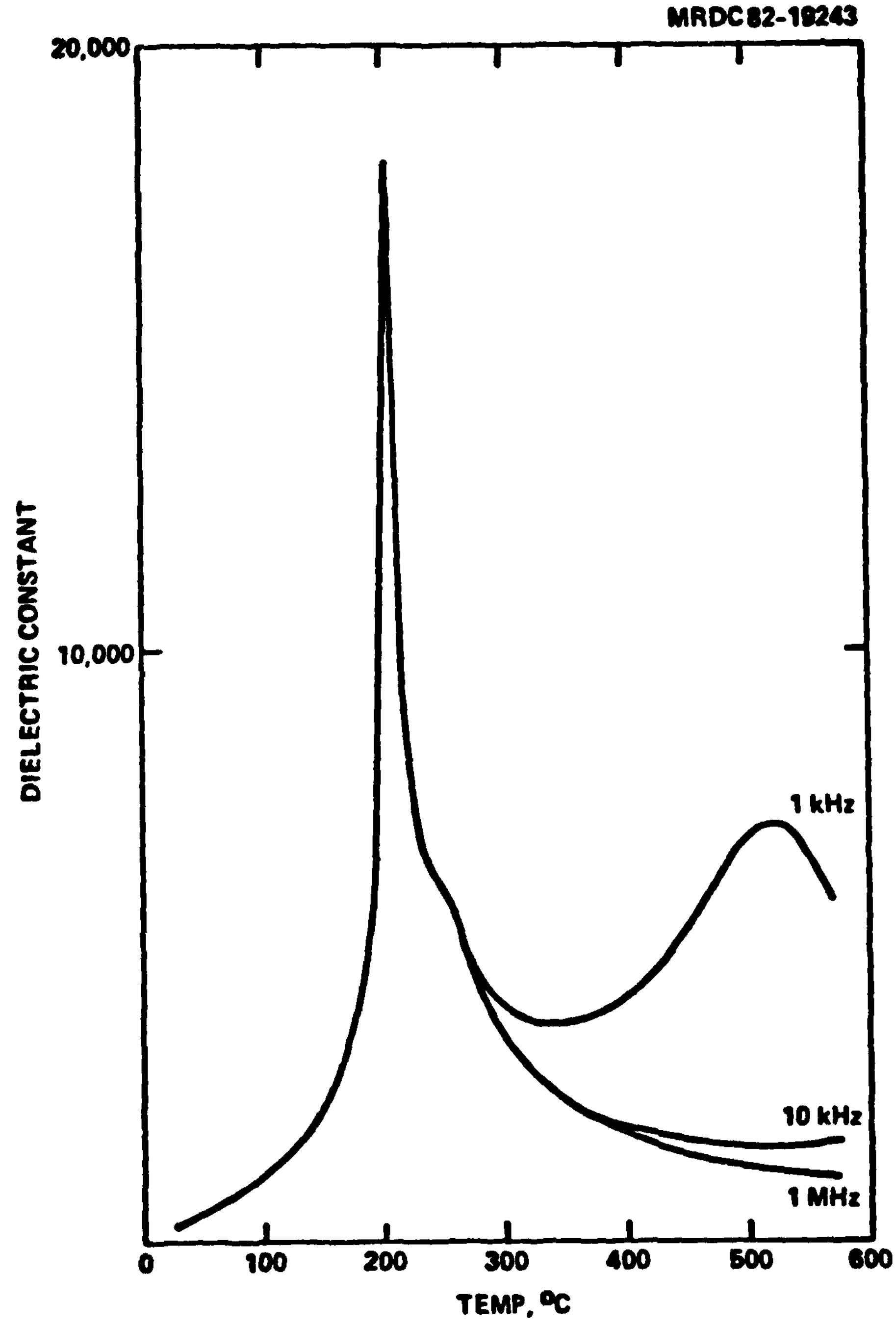

Fig. 3 Dielectric constant vs temperature for $Ba_{.2}Sr_{0.8}K_{0.7}Na_{0.25}Nb_5O_{15}$ single crystal, measured along (001) axis.

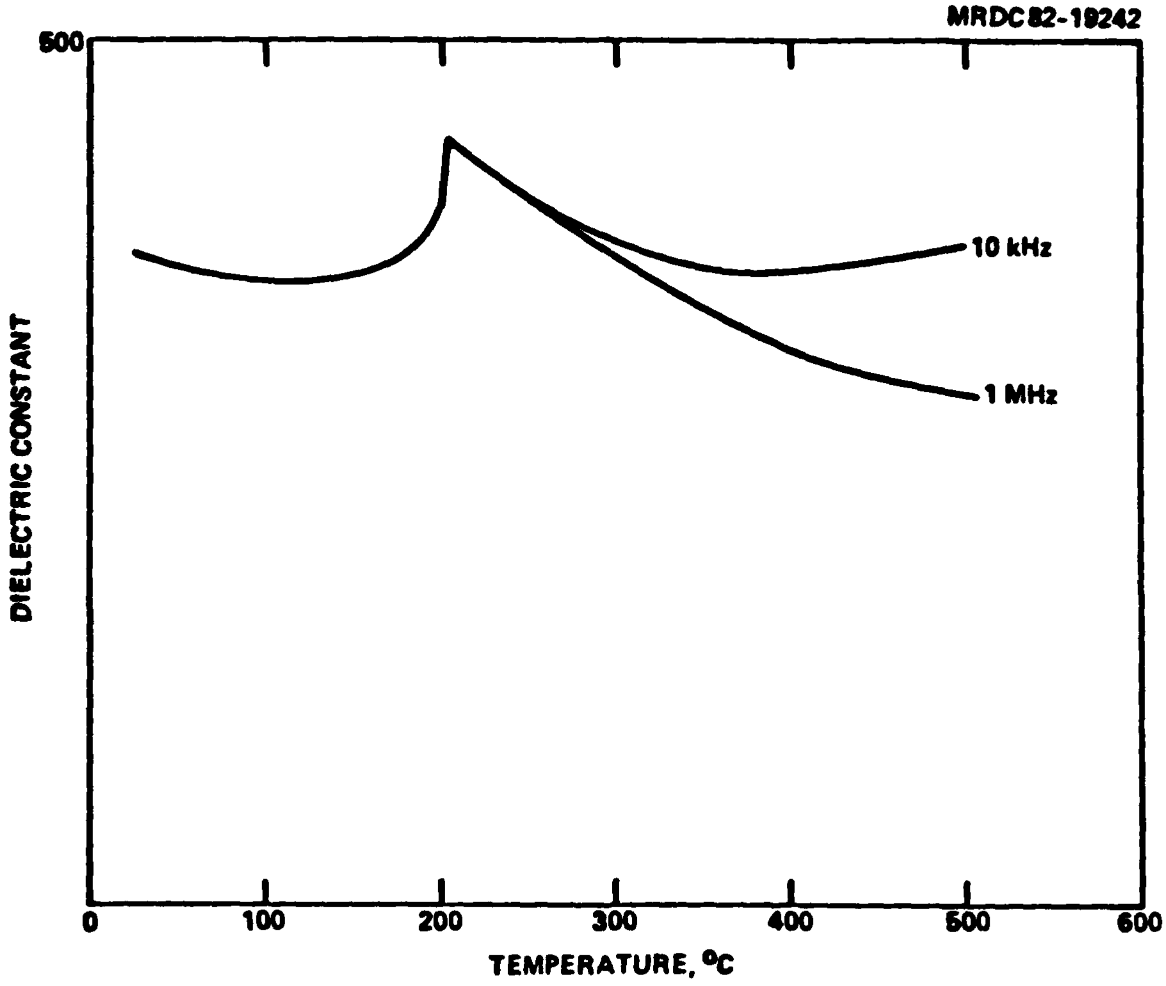

Fig. 4 Dielectric constant vs temperature for $Ba_{.2}Sr_{0.8}K_{0.7}Na_{0.25}Nb_5O_{15}$ single crystal, measured along (100) axis.

Powder x-ray diffraction data for this material show a tetragonal structure with lattice constants $a_{\AA} = 12.51$ and $c_{\AA} = 3.975$ for the $Ba_{1.2}Sr_{0.8}K_{0.75}Na_{0.25}Nb_5O_{15}$ composition. Congruent melting was found over the range of Sr_x composition $0.7 < x < 0.9$ examined thus far.

The electromechanical coupling coefficients k_{33} and k_{15} were evaluated for the $Ba_{1.2}Sr_{0.8}K_{0.75}Na_{0.25}Nb_5O_{15}$ composition using platinum electrodes. Single crystal samples were initially poled along the (001) axis in an oil bath at 165°C, but indications were that the samples were not completely poled at this temperature. However, poling in air at fields up to 7.5 kV/cm at temperatures beginning slightly above T_c give very encouraging results for k_{15} and k_{33}; these are summarized in Table 3 along with results for other tungsten bronze materials.

It is interesting to note from the data in Table 3 that the piezoelectric strain coefficient d_{15} for this large unit cell bronze composition is much greater than those observed for the smaller unit cell bronze crystals such as SBN. Similarly, its electromechanical coupling constants k_{33} and k_{15} are significantly larger than for other bronze compositions. It is clear from this data that low frequency dielectric constant and piezoelectric strain coefficient properties of BSKNN are strikingly different from the smaller unit cell bronze crystals, and this may play an important role in characterizing the high frequency dielectric properties of these materials.

Future work is planned for this crystal composition, specifically with regard to the optimum growth parameters for large diameter, crack-free material, and the further enhancement of the ferroelectric properties. This work will particularly focus on the material properties along the compositional pseudobinary join BKN-SNN, and the use of high-purity starting materials in crystal growth.

4.3 Ferroelectric Bronze Compositions Based on the $PbNb_2O_6$ Phase

Our millimeter wave measurements on the tungsten bronze SKN single crystal have already shown that high frequency dielectric constant along the non-polar axis is much higher than that along the polar c-axis. This is an

Table 3
Piezoelectric Properties of the Tungsten Bronze Compositions

Property	SBN	KLN	PBN (1)	PBN (2)	BSKNN
Structure	Tetra	Tetra	Tetra	Ortho	Tetra
Curie Temp (°C)	72	408	345	430	203
Dielectric Constant, K_{33}, at Room Temp.	800	80	200	1900	285
Coupling Coefficient					
k_{15}	0.13	0.35	----	----	0.28
k_{31}	0.14	0.18	0.22	----	----
k_{33}	0.47	0.54	0.55	----	0.47
k_{24}	----	----	----	----	----
Piezoelectric Stress Coefficient (c/m^2)					
e_{33}	4.30	5.50	----	----	----
e_{15}	2.0	4.6	----	----	----
e_{24}	----	----	----	----	----
Piezoelectric Strain Coefficient (1×10^{-12} C/N)					
d_{31}	-30.0	-14.0	-57	----	----
d_{33}	130	57	110	70	60
d_{15}	31	68	250	500	70
d_{24}	----	----	----	----	----

Compositions:

SBN = $Sr_{0.6}Ba_{0.4}Nb_2O_6$
PBN(1) = $Pb_{0.6}Ba_{0.4}Nb_2O_6$; PBN(2) = $Pb_{.87}Ba_{.20}Nb_2O_6$
KLN = $K_3Li_2Nb_5O_{15}$
BSKNN = $Ba_{1.2}Sr_{0.8}K_{0.75}Na_{0.25}Nb_5O_{15}$

interesting observation warranting further study and it is therefore worth considering a bronze composition where two polar directions are available. Lead metaniobate, $PbNb_2O_6$, belongs to the orthorhombic tungsten bronze structure[4,5] and possesses two polar directions, namely the c- and b-axes. However, the preparation of a pure $PbNb_2O_6$ phase is very difficult, and hence several substitutions in this phase have been accomplished to synthesize this material.[6,7,8] The addition of these additives has also enhanced the dielectric and piezoelectric properties for these solid solution systems.

In the present program two systems, $Pb_{1-x}Ba_xNb_2O_6$ and $Pb_{1-2x}K_xLa_xNb_2O_6$, have been selected and studied in detail. The substitution of barium and K + La first decreases the orthorhombic distortion, and then induces a tetragonal structure with the polar axis along the c-axis rather than orthorhombic c- and b-axes. This phase is tetragonal both above and below the Curie point, with large discontinuity in cell parameters at the Curie transition. The substitutional amounts of Ba^{2+} and K + La in $PbNb_2O_6$ causes remarkable changes in the ferroelectric properties of lead metaniobate.[9] These results are discussed in the following sections.

4.3.1 $Pb_{1-2x}K_xLa_xNb_2O_6$

The work on $K_{.5}La_{.5}Nb_2O_6$ by Soboleva et al[10] and our work on $K_{.5}Bi_{.5}Nb_2O_6$ show that these two phases crystallize in the tetragonal crystal symmetry and are isostructural with the high temperature tetragonal modification of $PbTa_2O_6$. At room temperature, the ferroelectric $PbTa_2O_6$ phase has an orthorhombic symmetry and is isostructural with the tungsten bronze $PbNb_2O_6$ phase. This suggests that all the systems considered here are structurally related and should form a continuous solid solution on the pseudobinary systems $PbNb_2O_6$-$K_{.5}Nb_2O_6$ and $PbNb_2O_6$-$K_{.5}Bi_{.5}Nb_2O_6$. The results of x-ray diffraction powder work are in good agreement, and a complete solid solution has been identified in both of the systems. Three structurally related phases, namely, the orthorhombic and the tetragonal tungsten bronze type phases and tetragonal $K_{.5}La_{.5}Nb_2O_6$, have been established for the $Pb_{1-2x}K_xLa_xNb_2O_6$ solid solution system.

The results of x-ray measurements at room temperature show a homogeneity range of orthohombic $Pb_{1-2x}K_xLa_xNb_2O_6$ to $x = 0.47$, while the tetragonal tungsten bronze phase is present in the composition range $0.48 < x < 0.85$. At the other end, the crystalline solid solubility of $PbNb_2O_6$ in the $K_{.5}La_{.5}Nb_2O_6$ phase is limited and is estimated to be in the composition range $0.86 < x < 1.0$. At the composition $x = 0.47$, both the orthorhombic and tetragonal tungsten bronze phases coexist. The variation of lattice parameters as a function of composition for the system $Pb_{1-2x}K_xLa_xNb_2O_6$ is shown in Fig. 5. The a and c parameters increase only slightly, while the b parameter decreases considerably with increasing concentration of $K_{.5}La_{.5}Nb_2O_6$ in the $PbNb_2O_6$ phase. The decrease in the b parameter is substantial compared to the a parameter, so that the ratio b/a becomes close to unity for values $x < 0.50$.

Typical data for the dielectric constant vs temperature for sintered ceramic disks are shown in Fig. 6 for a few compositions in the $Pb_{1-2x}K_xLa_xNb_2O_6$ system. It can be seen that the dielectric constant decreases and broadens whereas the room temperature dielectric constant increases with increasing K^+ and La^{3+} up to $x = 0.40$. Furthermore, the ferroelectric phase transition temperature T_c is shifted towards a lower temperature with increasing amounts of $K_{.5}La_{.5}Nb_2O_6$ in $PbNb_2O_6$. T_c for pure $PbNb_2O_6$ has been recorded at 560°C,[4,11] and this temperature drops with the addition of K^+ and La^{3+} or Bi^{3+} in both the orthorhombic and the tetragonal tungsten bronze phases. By using this peak position, the transition temperature for each system has been determined. Figure 7 shows the variation of T_c as a function of composition for $Pb_{1-2x}K_xLa_xNb_2O_6$ as well as the $Pb_{1-2x}K_xBi_xNb_2O_6$ system. Variation of T_c with composition is linear in both systems and is approximately of the same order. Lowering of T_c has also been reported for several other systems based on the $PbNb_2O_6$ solid solutions.

Table 4 summarizes the physical constants for the $Pb_{1-2x}K_xLa_xNb_2O_6$ system. Although the system $Pb_{1-2x}K_xBi_xNb_2O_6$ has also been investigated in these laboratories, this system does not possess physical properties as favorable as PKLN in this work. As can be seen in Table 4, the dielectric constant of PKLN increases significantly with the addition of $K_x + La_x$ in the othorhombic tungsten

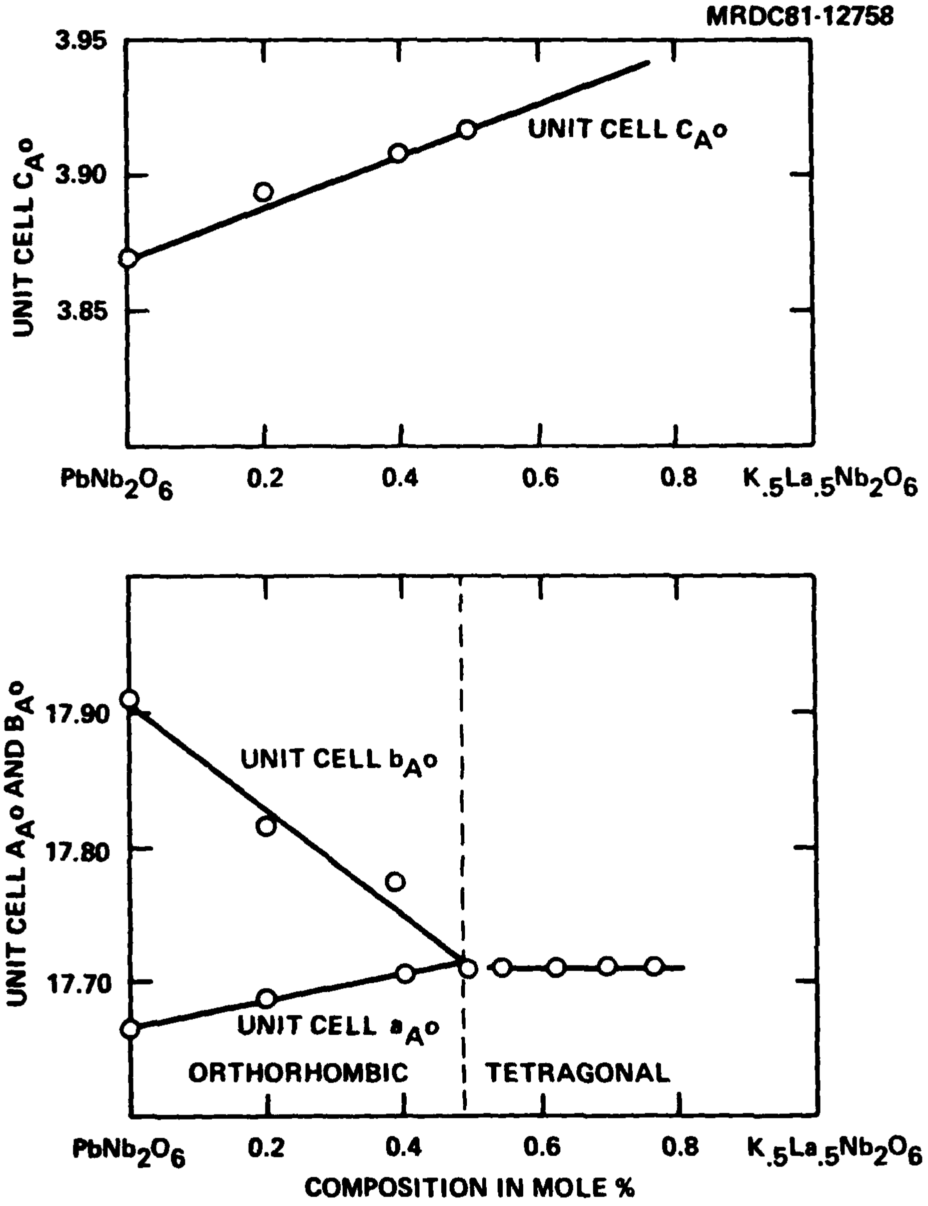

Fig. 5 Variation of lattice parameters for the $Pb_{1-2x}K_xLa_xNb_2O_6$ solid solution.

MRDC82-17598

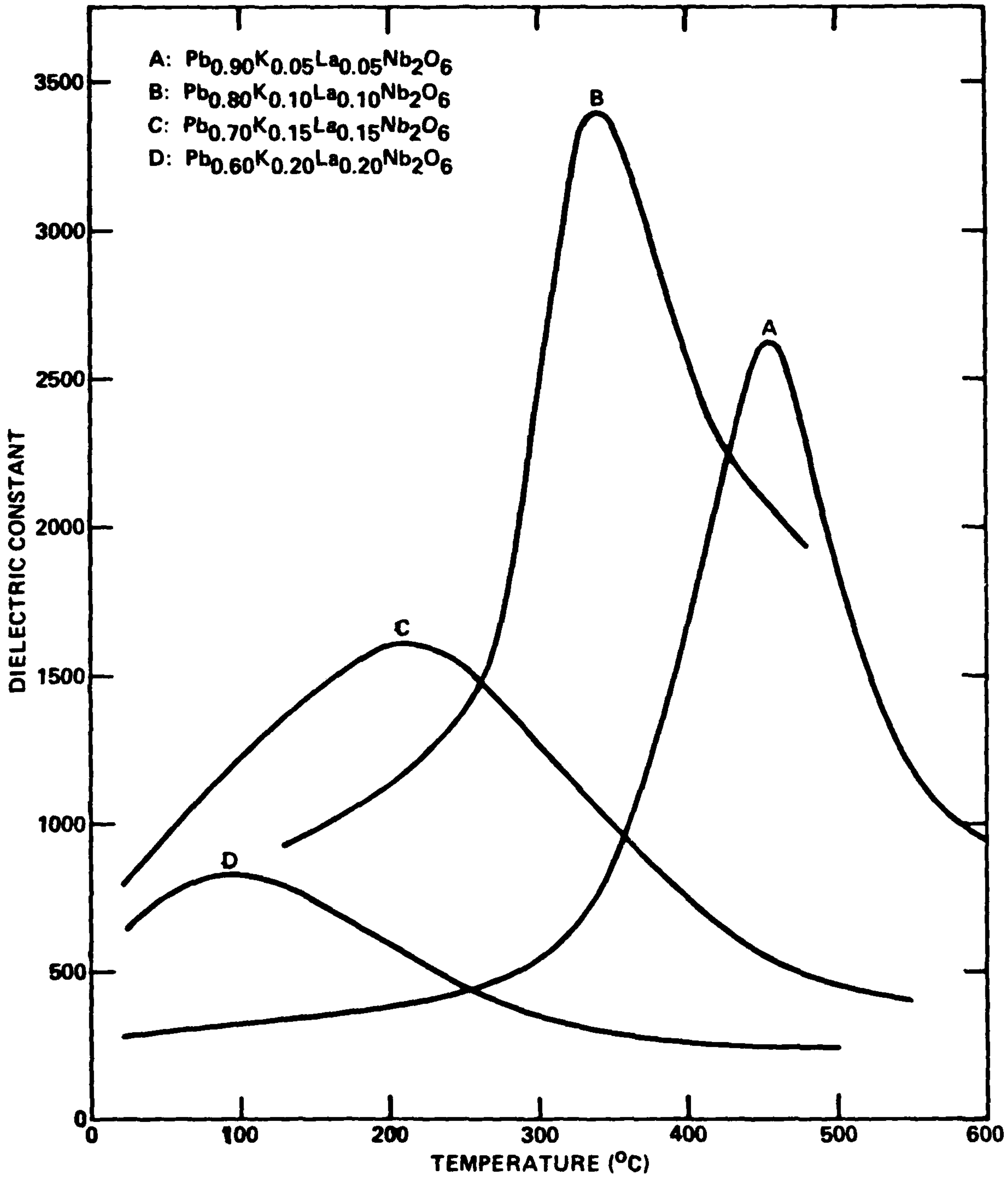

Fig. 6 Dielectric constant vs temperature of $Pb_{1-2x}k_xLa_xNb_2O_6$.

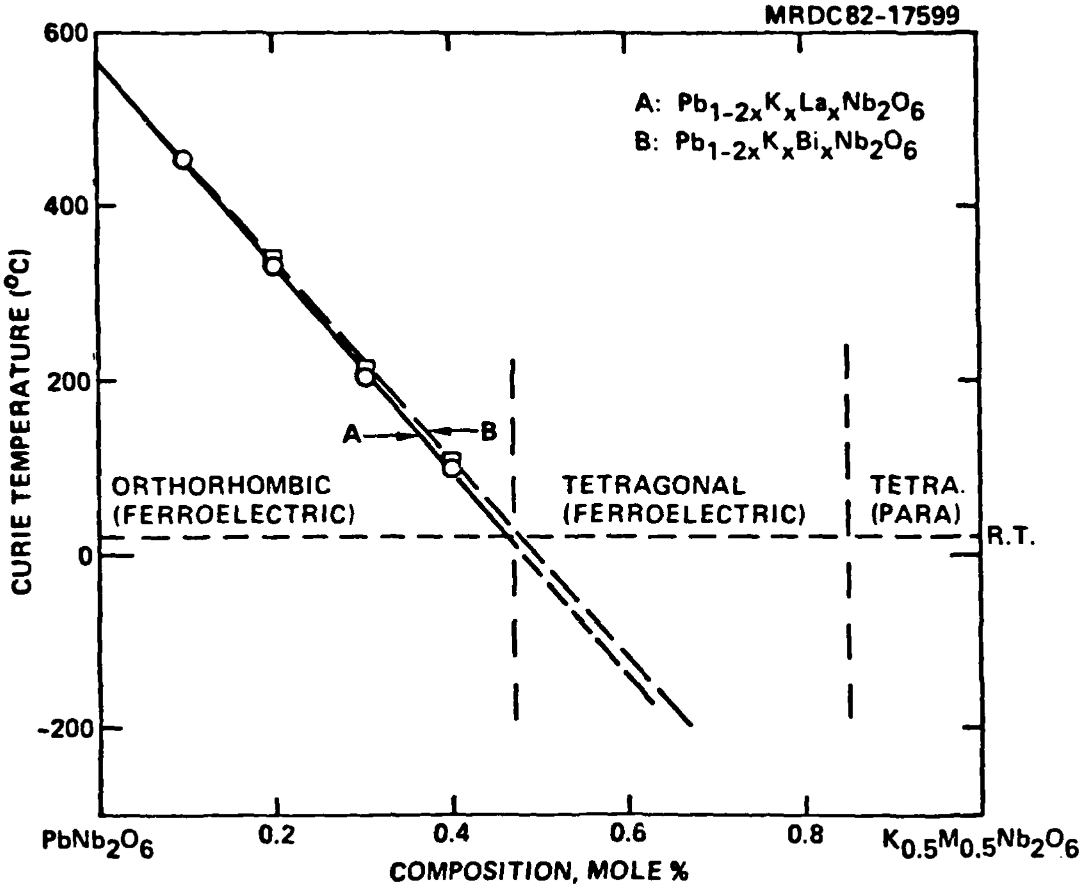

Fig. 7 Variation of ferroelectric transition temperature for the $Pb_{1-2x}K_xM_x^{3+}Nb_2O_6$ system, M = La or Bi.

bronze phase, with a maximum at x = 0.10. The piezoelectric strain coefficient (d_{33}) measurements on various samples were performed using the Berlincourt d_{33}-meter and the results of this study indicate that the composition $Pb_{.8}K_{.1}La_{.1}Nb_2O_6$ again shows the optimum d_{33} coefficient for this system. We believe these values may increase substantially if poling is achieved at higher temperatures. In the present case, poling was accomplished in a silicon oil bath at approximately 150°C, which is a very low temperature compared to the respective Curie temperatures. It is anticipated that by improving the poling technique for these ceramic samples it will be possible to better establish the d_{33} coefficient. In any case, the present piezoelectric strain coefficient value obtained for $Pb_{.8}K_{.1}La_{.1}Nb_2O_6$ is much higher than that reported for $PbNb_2O_6$ crystals,[12] indicating that this composition can find use for piezoelectric transducer and high frequency dielectric applications.

Table 4 also shows preliminary data for hot-pressed $Pb_{.8}K_{.1}La_{.1}Nb_2O_6$. This dense ceramic was formed by hot-pressing at 1280°C for two hours with a uniaxial pressure of 4000 psi. Sample slices were then oxidized for 2 hours at

Table 4
Physical Constants for Orthorhombic
$Pb_{1-2x}K_xLa_xNb_2O_6$

Composition	Curie Temp T_c, °C	Dielectric Constant, K		Piezoelectric Strain Coeff. d_{33}, c/n
		R.T.	T_c	
$PbNb_2O_6$	560	-	-	100×10^{-12}
$Pb_{.90}K_{.05}La_{.05}Nb_2O_6$	455	280	2610	-
$Pb_{.80}K_{.10}La_{.10}Nb_2O_6$	339	720	3390	130×10^{-12}
$Pb_{.80}K_{.10}La_{.10}Nb_2O_6$ (HP)*	333	665	4820	-
$Pb_{.70}K_{.15}La_{.15}Nb_2O_6$	201	790	1600	106×10^{-12}
$Pb_{.60}K_{.20}La_{.20}Nb_2O_6$	98	650	830	-

All samples sintered ceramics except for (*), which is hot-pressed.

1100°C prior to measurement. Cracking of the ceramic during hot-pressing has been a significant problem to date because of the orthorhombic structure of the material and a possible second phase transition above 1150°C. Nevertheless, dielectric data for the dense ceramic shows that the low frequency (10 kHz) dielectric constant at T_c is 40% greater than for the equivalent cold-pressed and sintered material. Although the hot-pressed material shows a slightly lower room temperature value for the dielectric constant, the dielectric losses are somewhat better, being ~ 0.02 at 1 MHz. These are encouraging results, and certainly warrant continued work on the optimization of the hot-press procedures for this material.

In the case of the $Pb_{1-x}Ba_xNb_2O_6$ system to be discussed in the next section, the substitution of Ba^{2+} (1.50Å) for Pb^{2+} (1.32Å) first decreases the orthorhombic distortion, and then induces a tetragonal structure with the polar axis along the c rather than along the b axis.[6,7] Further, the interesting feature in this system is that T_c first decreases in the othorhombic tungsten bronze phase and then increases in the tetragonal tungsten bronze phase. Since the average ionic size of $K^+ + La^{3+}$ (1.355Å) is bigger than Pb^{2+}, and since both systems, $Pb_{1-2x}K_xLa_xNb_2O_6$ and $Pb_{1-x}Ba_xNb_2O_6$, are structurally similar, it was expected that the addition of K^+ with La^{3+} would produce similar results, i.e., first a decrease and then an increase in the T_c. The results of this investigation (Fig. 7) indicate that a continuously decreasing Curie temperature occurs with increasing amounts of $K^+ + La^{3+}$ or $K^+ + Bi^{3+}$ in both the orthorhombic and tetragonal tungsten bronze phases, indicating that T_c is not only controlled by the size of substituent ions, but its location in the structure is equally important. Since the coordination of Pb^{2+} is 15- and 12- fold in the tungsten bronze structure, there exists three possibilities for each ion in this structure, namely in the 15 or 12, or in both sites. Neither the work reported in the literature nor the results of this investigation are sufficient to establish the ionic site preference or their distribution over the two crystallogrphic sites. Further work in this direction is of significant interest in the present study in order to establish the site preference for different ions and their influence over the T_c behavior and the ferroelectric properties.

4.3.2 $Pb_{1-2x}Ba_xNb_2O_6$

The second lead-containing composition studied in this work is the system $Pb_{1-2x}Ba_xNb_2O_6$ (PBN). Ceramic and single crystal growth and characterization of this material was initiated at the Pennsylvania State University with the aim of achieving crystals of sufficient size and quality for dielectric and piezoelectric characterization.[13] Although some small (5-8 mm diameter) crystals have been successfully grown, cracking and excessive lead loss during Czochralski growth indicate the need for alternative growth techniques for this interesting and potentially useful material. Therefore, we have initiated work on the growth of hot-pressed dense ceramic PBN with the aim of avoiding many of the problems associated with single crystal growth.

Initial work on PBN shows this material to have both orthorhombic and tetragonal forms depending on its composition, with a morphotropic phase boundary occurring at $x = 0.37$. Measurements of the Curie temperature T_c vs composition are shown in Fig. 8. Concurrent theoretical modeling work on this material[13] has predicted very high values for the dielectric constant and the piezoelectric strain coefficient d_{15} for compositions near the morphotropic phase boundary between the ferroelectric orthorhombic (mm2) and tetragonal (4mm) structures. Therefore, our initial work has focussed on the tetragonal composition $Pb_{.60}Ba_{.40}Nb_2O_6$ with the addition of 2% substitutional La in order to enhance the optical properties of the hot-pressed ceramic material.[14] Current growth conditions, using graphite die sets in an N_2 atmosphere, are 4000 psi uniaxial pressure and a growth temperature of 1240-1280°C for two hours. The 1 inch diameter disks are then sliced and oxidized for 2-4 hours at 1100°C, resulting in translucent, pale yellow to white-colored ceramic material. The mechanical quality of the hot-pressed PBLN samples is excellent, and the samples are free of any significant cracking.

Low frequency dielectric measurements on hot-pressed $(Pb_{.60}Ba_{.40})_{.97}La_{.02}Nb_2O_6$ (PBLN 60/40/2) show evidence of grain orientation along the c-axis perpendicular to the axial pressure, with dielectric constant

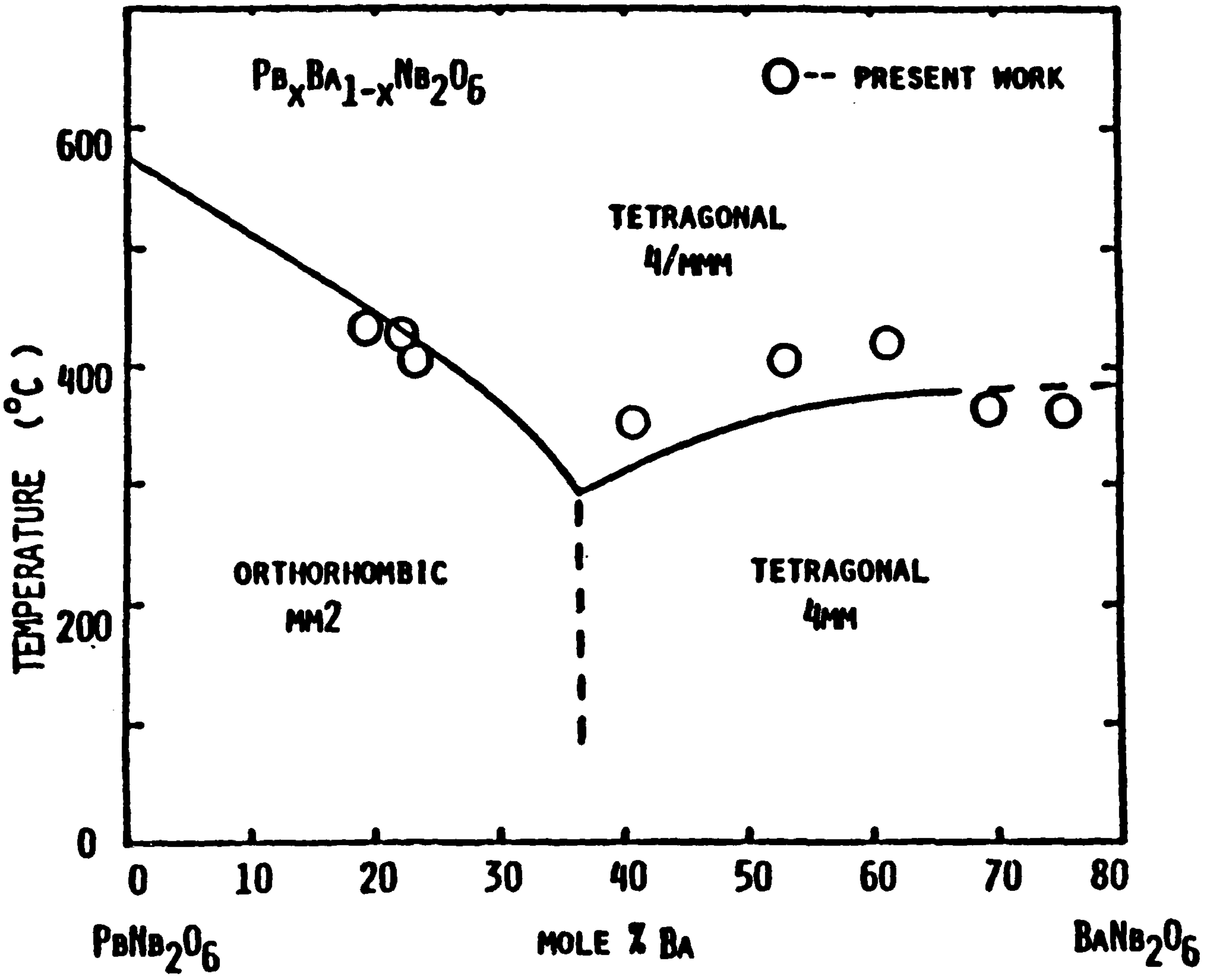

Fig. 8 Phase diagram for ferroelectricity in the solid solution system $Pb_{1-x}Ba_xNb_2O_6$.

ratios for face normals perpendicular and parallel to the axial pressure of up to 1.8:1. Typical dielectric constant values at 10 kHz for perpendicular-cut samples are 2300 at room temperature and 8000 at $T_c = 230°C$, a temperature lower than predicted in Fig. 8 due to the addition of 2% La.[14,15] Although present room temperature dielectric losses are high, rising from .02 at 1 kHz to .07 at 1 MHz, these preliminary results are exceptionally promising for potential millimeter wave applications of this material. It is planned to continue work on PBN/PBLN hot-pressed ceramics and further investigate the ternary PbO-BaO-Nb_2O_5 phase diagram for this material in order to determine the effect of compositional changes on the dielectric properties.

5.0 TUNGSTEN BRONZE FAMILY: MILLIMETER WAVE PROPERTIES

5.1 Measurements on BSKNN

Several single crystal samples of BSKNN cut to fill the waveguide cross-section were studied from 30-40 GHz and from 90-100 GHz. Power reflection and transmission coefficients were measured in each band of frequencies and complex permittivities $\varepsilon' + i\varepsilon''$ were determined by fitting to these measured values. Tables 5.1 - 5.4 summarize the results of this procedure at selected frequencies in each band for the two polarizations of the microwave electric field, namely parallel and perpendicular to the crystal polar (c-) axis.

In Table 5.2 results are given for the perpendicular permittivity on two samples cut from the same boule. The sample-to-sample variability shown here is fairly typical. In the higher frequency band, four samples were measured for each polarization (results for a-axis sample #2 are omitted from Table 5.4 for reasons discussed below). All samples show substantial decrease in their real permittivity from the values at 30 GHz, accompanied by increases in the loss tangent $\tan\delta = \varepsilon''/\varepsilon'$, primarily due to the decrease in ε'.

The fit for a-axis sample #2 between 90 and 100 GHz did not produce a unique value for the permittivity, due to an unfortunate convergence of roots in the expressions for the reflected and transmitted power. Values of ε' ranging from 200 to 500 gave equally valid fits. Values for ε'' were more grouped, and showed a definite increasing trend within the band, ranging from about 30 ± 3 at 92 GHz to 40 ± 5 at 98 GHz.

5.2 Measurements on PKLN

Sintered ceramic samples of $Pb_{.70}K_{.15}La_{.15}Nb_2O_6$ (PKLN 70/30) and $Pb_{.80}K_{.10}La_{.10}Nb_2O_6$ (PKLN 80/20) cut parallel and perpendicular to the pressing axis were studied from 30 - 40 GHz. Such high losses were observed ($\tan\delta \sim 0.5$) that measurements at higher frequency were not deemed worthwhile at present. Results for ε' and ε'' at 35 GHz are given in Table 6 for all four samples.

Table 5
Dielectric Data for BSKNN at Millimeter Wave Frequencies

Table 5.1
BSKNN - c-Axis

f, GHz	ε'	ε"
30	360	10.9
33	300	16.4
36	265	23.9
39	240	24.9

Table 5.2
BSKNN - a-Axis

	Sample #a		#b	
f, GHz	ε'	ε"	ε'	ε"
33	275	49.3	260	59.7
36	290	23.5	285	25.5
39	245	51.4	285	22.6

Table 5.3
BSKNN c-Axis

f, GHz	Sample #1		#2		#3		#4	
	ε'	ε"	ε'	ε"	ε'	ε"	ε'	ε"
92	57	10.4	56	9.95	52.5	11.5	50	12.7
94	54	11.3	54	10.8	50	11.2	50	12.8
96	52	11.2	52	10.9	50	10.5	57.5	13.7
98	50	11.3	50	10.9	55	10.1	55	13.1

Table 5.4
BSKNN a-Axis

f, GHz	Sample #1		#3		#4	
	ε'	ε"	ε'	ε"	ε'	ε"
92	47.5	27.4	95	26.7	93	28.7
94	55	34.2	95	30.0	108	34.8
96	60	35.9	100	29.2	100	36.7
98	70	34.0	100	26.1	100	35.9

Some degree of anisotropy in ε' is evidenced in the table, but ε" is near 50 in all cases. The values of ε' between 70 and 150 should be compared with low-frequency values on the same material between 650 and 800.

Table 6
Dielectric Data for Sintered PKLN at 35 GHz

	ε'	ε"
70/30 parallel	108	51
70/30 perpendicular	73	46
80/20 parallel	146	63
80/20 perpendicular	102	62

5.3 Interpretation

The most striking feature of the millimeter wave measurements on tungsten bronze ferroelectrics to date is the high loss and dispersion in dielectric properties compared with the low frequency behavior of these same materials. The Devonshire model which fits this low frequency behavior is generally understood to reflect the dominance of a single soft mode in the dielectric response; this mode residing above 1000 GHz at room temperature and moving into the measurement range as the Curie point is approached.

There is no room in such a model for a rapid dispersion in the GHz range at room temperature. The observed behavior is suggestive of piezoelectric resonance, spread over a broad frequency range by a corresponding spread in the characteristic dimension of the resonating regions. Such regions might be microdomains stabilized by localized defects. However, one would then expect sensitivity of the high-frequency loss to the details of the poling procedure, and this is not observed. Losses in poled and unpoled samples of SBN were found to be indistinguishable.

Another possibility, which we are only now in the process of exploring, is that growth defects can themselves provide a strong, non-resonant piezoelectric coupling to heavily damped elastic waves. It has long been known that high-frequency acoustic waves in soft-mode ferroelectrics are strongly attenuated.[16] If dislocations in the ferroelectric produce large local gradients in the polarization, the microwave electric field can drive these dislocations to produce acoustic radiation. In the most favorable case, the rate of dissipation by this process can approach half the maximum resonant loss in the same volume of material.

6.0 FUTURE PLANNED WORK

1. Improve the current Czochralski bulk growth technique to develop large sized (approximately 1 to 2 cm in diameter) $Ba_{2-x}Sr_xK_{1-y}Na_yNb_5O_{15}$ (BSKNN) crystals of optical quality. If needed, the Sr:Ba or K:Na ratio will be changed to obtain the optimum composition for high frequency studies.

2. Continue to improve the hot-pressing technique for the $Pb_{1-2x}K_xLa_xNb_2O_6$ solid solution system, for both the orthorhombic and tetragonal bronze compositions.

3. Initiate phase relation and preparation of dense samples for the $Pb_{1-2x}Ba_xNb_2O_6$ solid solution system. Initially the compositions close to the morphotropic region will be studied since they exhibit interesting dielectric properties.

4. Carry out structure factor analysis to identify the site preference for various cations, specifically on the 15 and 12-coordinated sites, and their role in improving the ferroelectric properties.

5. Initiate Transmission Electron Microscopy (TEM) analysis work on the selected bronze compositions to establish the kinds of defects present in the crystals.

6. Measure millimeter wave dielectric properties of selected low-defect ferroelectric materials to test defect-based models for the loss mechanism.

7. Calculate frequency-dependent complex permittivities predicted by postulated loss mechanisms.

7.0 PUBLICATIONS AND PRESENTATIONS

7.1 Publications

1. R. R. Neurgaonkar, W. W. Ho, W. K. Cory, W. F. Hall and L. E. Cross, "Low and High Frequency Dielectric Properties of Ferroelectric Tungsten Bronze $Sr_2KNb_5O_{15}$ Crystals," submitted to Ferroelectrics.
2. R. R. Neurgaonkar, J. R. Oliver, W. K. Cory and L. E. Cross, "Structural and Dielectric Properties of the Phase $Pb_{1-2}K_xLa_xNb_2O_6$, M = La or Bi," submitted to Mat. Res. Bull.
3. R. R. Neurgaonkar, W. K. Cory and J. R. Oliver, "Single Crystal Growth and Ferroelectric Properties of Tungsten Bronze $Ba_{2-x}Sr_xK_{1-y}Na_yNb_5O_{15}$ Crystals," submitted to Mat. Res. Bull.
4. W. W. Ho, W. F. Hall and R. R. Neurgaonkar, "Dielectric Properties of Ferroelectric Tungsten Bronze $Ba_{2-x}Sr_xK_{1-y}Na_yNb_5O_{15}$ Crystals at RF and Millimeter Wave Frequencies," to be submitted to Ferroelectrics.

7.2 Presentations

1. J. R. Oliver, R. R. Neurgaonkar and L. E. Cross, "Structural and Dielectric Properties of $Pb_{1-2x}K_xLa_xNb_2O_6$," to be presented at the Annual Meeting of American Ceramic Society in Chicago, April, 1983.
2. R. R. Neurgaonkar, W. K. Cory and J. R. Oliver, "Growth and Applications of Ferroelectric Tungsten Bronze Family Crystals," to be presented at the 1983 IEEE International Symposium on Applications of Ferroelectrics, June 1-3, 1983, NBS, Gaithersburg, Maryland.
3. W. W. Ho, W. F. Hall and R. R. Neurgaonkar, "Dielectric Properties of Ferroelectric Tungsten Bronze $Ba_{2-x}Sr_xK_{1-4}Na_yNb_5O_{15}$ Crystals at RF and Millimeter Wave Frequencies," to be presented at the 1983 IEEE International Symposium on Applications of Ferroelectrics, June 1-3, 1983, NBS, Gaithersburg, Maryland.

4. R. R. Neurgaonkar, J. R. Oliver and L. E. Cross, "Growth and Applications of Ferroelectric Tungsten Bronze Family Crystals," to be presented at the 5th European Meeting on Ferroelectricity, Malaga, Spain, Sept. 26-30, 1983.

8.0 REFERENCES

1. Landolt-Bernstein, Vol. 3 (1969); Vol. 9 (1973); Vol. 16a (1980), Ferroelectric and Antiferroelectric Substances, Ed. T. Mitsui, Springer Verlag, New York.
2. J. Ravez, A Perron Simon, P. Hagenmuller, Ann. Chem. 1:251 (1976).
3. R. R. Neurgaonkar, Semiannual Technical Report No. 2, Contract No. F49620-78-C-0093.
4. G. Goodman, J. Am. Ceram. Soc. 36, 368 (1953).
5. E. C. Subbarao and J. Hirazo, J. Am. Ceram. Soc. 45, 528 (1962).
6. E. C. Subbarao, G. Shirane and F. Jona, Acta. Cryst. 13, 226 (1960)
7. M. H. Francombe, Acta. Cryst. 13, 131 (1960).
8. P. Baxter and N. J. Hellicar, J. Am. Ceram. Soc. 43, 578 (1960).
9. E. G. Bronnikova, I. M. Larinov, N. D. Mileikovskaya, E. G. Smazhevskaya and I. A. Glozman, Izv Akad, Nauk. SSSR, Ser. Fiz. 24, 1440 (1960).
10. L. V. Soboleva and F. I. Dmitrieva, Inorg. Mat. 6, 1761 (1970).
11. G. Goodman, Am. Ceram. Soc. Bull. 31, 113 (1952).
12. B. Lewis and L. A. Thomas, Proc. Int'l. Conf. Solid State Phys., Electronics Telecomm., Brussels 4, Pt. 2, 883 (1960).
13. R. R. Neurgaonkar and L. E. Cross, Final Report, Contract No. F49620-78-C-0093 (1982).
14. M. Yokosuka, Jap. J. Appl. Phys. 16, 379 (1977).
15. K. Nagata and K. Okazaki, Japan-U.S. Study Sem. on Dielect. and Piezoelect. Ceram., Tokyo, No. W-11 (1982).
16. H. H. Barrett, in W. P. Mason and R. N. Thurston, Physical Acoustics, Vol. VI, p. 65.